ONECENTRAL PRESS

Available online at www.onecentralpress.com

One Central Press

OPEN ACCESS

journal homepage: www.onecentralpress.com/functional-nanostructures

Differentiation of Specific Cancer Biomarkers with Solid-state Nanopores

*Waqas Ali,[abc#] Muhammad Usman Raza,[abc#] Mohammed Arif I. Mahmood,[abc] Peter B. Allen,[d] Adam R. Hall,[e] Yuan Wan,[fg] and Samir M. Iqbal[*abchi]*

[a]*Nano-Bio Lab, University of Texas at Arlington, Arlington, TX 76019, USA. [*]E-mail address of corresponding author: SMIQBAL@uta.edu*
[b]*Department of Electrical Engineering, University of Texas at Arlington, Arlington, TX 76019, USA*
[c]*Nanotechnology Research Center, University of Texas at Arlington, Arlington, TX 76019, USA*
[d]*Department of Chemistry, University of Idaho, Moscow, ID 83844, USA*
[e]*Virginia Tech-Wake Forest School of Biomedical Engineering and Sciences, Wake Forest University School of Medicine, Winston-Salem, NC 27101, USA*
[f]*Ian Wark Research Institute, University of South Australia, Adelaide, South Australia 5095, Australia*
[g]*PMR Institute, Shanghai, China 201203*
[h]*Department of Bioengineering, University of Texas at Arlington, Arlington, TX 76019, USA*
[i]*Department of Urology, University of Texas Southwestern Medical Center at Dallas, TX 75390, USA* [#] *Equal Contribution*

ABSTRACT

Epidermal growth factor receptor (EGFR) is well known as an early biomarker for many cancer types. The sensitive and selective detection of EGFR can help in early diagnosis of cancer. We demonstrate a nanopore-based resistive pulse-sensing technique to selectively detect small amounts of EGFR from a mixture. An anti-EGFR aptamer was used to impart selectivity in the sample solution. The shift in translocation dwell time of samples, with and without a bound anti-EGFR aptamer, was used to detect EGFR. EGFR with the bound aptamer resulted in translocation dwell times that were about 23% shorter than those for EGFR alone, indicating a greater net charge for the complex. Thrombin was used as a control to demonstrate the high specificity of the aptamer for EGFR that enabled differentiation between similar-sized proteins. The use of anti-EGFR aptamer as a targeting agent makes the label free detection of EGFR possible without nanopore surface modification or functionalization.

I. INTRODUCTION

EGFR detection and enumeration promises early cancer detection [1, 2] and the ability to monitor therapy and prognosis [3-5]. Elevated levels of EGFR expression in patients' serum is a strong prognostic indicator for many tumor types [6-8]. For example, Quaranta *et al*. reported the mean EGFR level in brain cancer patients' sera to be nearly twice than that of healthy subjects [9]. The total concentration of EGFR in patient serum is very small (ng/ml) and can be easily obscured by the biological noise. These facts highlight two major challenges in detection of EGFR expression levels from patients' serum: first, a useful biosensor should have molecular level sensitivity, and second, it should have very high specificity. In last couple of decades, a variety of detection assays for proteins have been developed using fluorescence, electrochemical, colorimetric, chemiluminescence and surface plasmon resonance means [3, 10]. Many of these assays lack the sensitivity and specificity required for the quick detection of physiologically relevant EGFR levels. Enzyme-linked immunosorbent essay (ELISA) can detect in the range of ng/ml to pg/ml but it requires surface functionalization that has limited shelf-life and require sophisticated laboratory facilities.

Development of new approaches for point-of-care (POC) detection of protein biomarkers is a pressing need in early cancer diagnosis. Devices for POC must be ultrasensitive, fast, accurate, low priced and should be easy to use [11]. One candidate technology that has recently emerged as a potent single molecule detector is the solid-state nanopore [12-17] based on the resistive-pulse enumeration. When a molecule hinders the ionic flow through the nanopore, it registers a unique electrical pulse in the baseline ionic current trace. Analysis of these electrical pulses can be used to determine size and charge of molecules [12], length of nucleic acids [14, 18], protein size [19, 20], folding state [20, 21] and molecular agglomeration [22]. They can also be chemically modified [15, 23] for detection of specific biomarkers [17, 24] and toxic agents [25, 26].

Biological nanopores are unstable and their measurement setup is tedious due to their small fixed diameter (1.5 – 3.6 nm); only polypeptides or denatured proteins are able to translocate through these [27, 28]. Moreover, preparation of large-scale

protein nanopore arrays faces technical challenges [12]. On the contrary, solid-state nanopores are compatible with proteins of any conformation and size due to the tunable dimensions. These have been successfully used to detect proteins of various sizes and stochastic sensing of proteins [14]. The current approaches have some disadvantages. First, single-ligands functionalized nanopore can only detect one type of target protein; proteins not recognized by ligands are not detected at all. If several proteins need to be simultaneously identified, a number of ligands should be respectively immobilized on separate nanopores [29, 30]. This means multiple copies of samples and multiple sets of nanopore frameworks need to be prepared for signal collection, analysis and calibration. Although technically feasible, such strategies for multiplexed protein detection require tremendous workload and would be unreliable from the noise and system artifacts. In addition, due to different sizes of proteins, the nanopore diameters would need to be precisely tuned in order to accommodate each analyte. If the proteins of interest have broad range of sizes, that would be another challenge to decide on nanopores with suitable diameters. Another challenge is the immobilization of the specific ligands onto the inner walls of the nanopore. Surface functionalization at such small size scales is not trivial and is expected to result in insufficient immobilization sites and heterogeneous grafting especially when irregular surfaces result into various charge distributions and variations in the nanopore stoichiometry [12, 29, 30]. An ideal solid-state nanopore system should be able to simultaneously and quickly identify target proteins in a multiplexed fashion from a single miniscule sample (Fig. 1 (a)). Such detection should be performed, from initial system setup to final data report, on one framework.

This paper reports solid-state nanopores as single-molecule sensors [31-33] for detection and enumeration of EGFR at POC settings. To keep the process simple, instead of using a functionalized nanopore [34], a bare nanopore was used and in-solution binding of EGFR with anti-EGFR aptamer was used to impart selectivity [35]. Anti-EGFR aptamer is very selective and has high affinity for EGFR [36]. Aptamer binding to the protein altered the overall charge and mass of the complex as compared to the unbound EGFR [37]. Since the speed of the translocating species strongly depended upon its charge [38-40], attachment with aptamer altered the translocation time for EGFR. This change was readily identified from the analysis of registered pulses. As a negative control, the experiments were done with human α-thrombin protein. With thrombin, no change was observed in the translocation time after incubating the protein with the anti-EGFR aptamer.

II. RESULTS AND DISCUSSION

Current-voltage (*I-V*) characteristics of the nanopore in 20 mM Tris-acetate (pH 8.2) + 5 mM Mg-acetate + 1 mM K-acetate are shown in Figure 1(b). Conductance of the nanopore was found to be 2.5 μS by a linear fit to the data. For the voltage range of -100 mV to +100 mV, linear *I-V* characteristics were observed [41, 42]. Open pore current for the nanopore at 50 mV applied bias is shown in Figure 2(a).

EGFR was introduced into the negative side of the nanopore. EGFR translocation resulted in significant current blockage events. A snapshot of the nanopore current trace with EGFR is shown in Figure 2(c). These pulses were recorded at 50 mV bias applied across the nanopore. Very uniform current pulses were observed in terms of translocation time and peak amplitude.

Table 1 Pulse statistics for unbound EGFR and EGFR-aptamer complex.

Translocating Species	Translocation Time [μs]	Peak Amplitude [nA]
EGFR (Unbound)	80 ± 4.06	0.9 ± 0.21
EGFR-Aptamer Complex	62 ± 5.24	1.1 ± 0.18

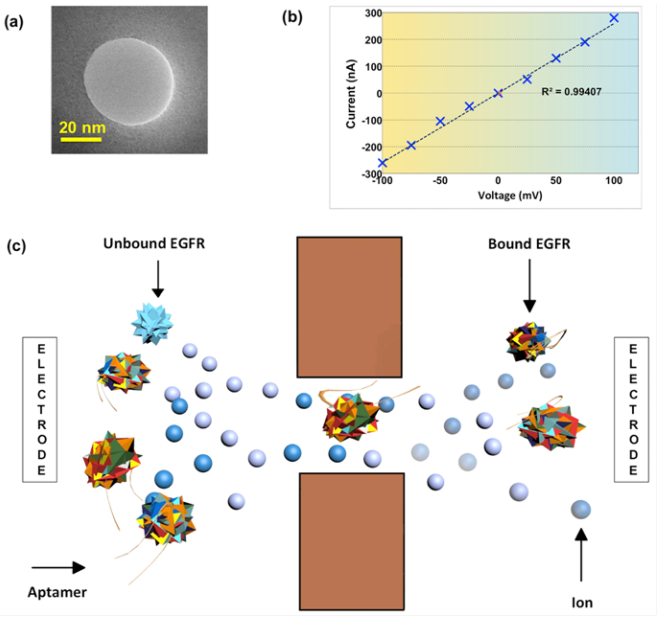

Figure 1 Nanopore for EGFR translocation experiments. (a) Transmission Electron Microscope (TEM) micrograph of a 40 nm diameter solid-state nanopore fabricated in 40 nm thick freestanding SiN membrane drilled with focused electron beam of TEM. (b) Linear *I-V* characteristics for the nanopore show 2.5 μS conductivity. (c) Incubating EGFR with aptamer allows them to bind with EGFR molecules and form the complex. Complex has higher charge and is slightly larger. The pulses from complex are shorter in width but deeper when compared to those registered by unbound EGFR.

EGFR translocation through the nanopore registered characteristic current pulses with average peak amplitude of 0.9 ± 0.21 nA and average translocation time of 80 ± 4.06 μs (Table 1). Only one population of events was observed for the peak amplitude *versus* the translocation time for EGFR

translocation through nanopore at 50 mV as shown in Figure 2(d).

In the next set of experiments, again EGFR was introduced into the negative side of the nanopore for translocation but this sample was incubated with anti-EGFR aptamer for a certain period. The conditions of EGFR and anti-EGFR aptamer incubation are given in the experimental section. This time again, significant current blockage events were observed. There were, however, two distinct types of pulses now (Figure 3(a)). The two types of pulses were not very different in terms of their peak amplitudes but they were remarkably different in terms of their translocation times. The two types of pulses were different from each other by 22.5% with respect to their average translocation times and 18.2% in terms of their average peak amplitudes.

One of the two types of pulses were exactly similar (i.e. same translocation time and peak amplitude) to those that were observed for EGFR-only translocation. The second type of pulses had shorter widths i.e. higher translocation speed, and larger peak amplitudes i.e. more pore blockage, when compared to those for pulses associated with EGFR translocation without incubation with the aptamer. The second type of pulses stemmed from the translocation of the complex. The complex translocation through a 40 nm wide and 40 nm thick solid-state nanopore under an applied voltage of 50 mV registered pulses with average peak amplitude of 1.1 ± 0.18 nA and average translocation time of 62 ± 5.24 µs. The presence of two distinct types of populations can be clearly seen in Figure 3(d). Another important point to notice from this scatter plot is that the events frequency is not the same for the two types of pulses. There are much more events of EGFR translocation as compared to that of complex translocation. One plausible reason for that could be the abundance of unbound EGFR as compared to the EGFR-aptamer complex. To systematically prove this hypothesis, a titration series was conducted in which the molar concentration of EGFR was kept constant and the molar concentration of anti-EGFR aptamer was gradually increased. Figures 3(b) and 3(c) show the 10 sec current traces when EGFR was incubated with 4 µM and 10 µM anti-EGFR aptamer, respectively. For each case, blockage events are plotted on a scatter plot of translocation time *versus* peak amplitude (Figures 3(e) and 3(f)). A gradual increase in the event frequency for complex translocation was observed as the molar concentration of aptamer increased. The effect was opposite on the event frequency of EGFR translocation. It kept on decreasing. This shifting signal from event population of EGFR to that of complex, with the increase in aptamer concentration, indicated that many more EGFR molecules were binding to aptamer and forming complexes as the aptamer concentration increased.

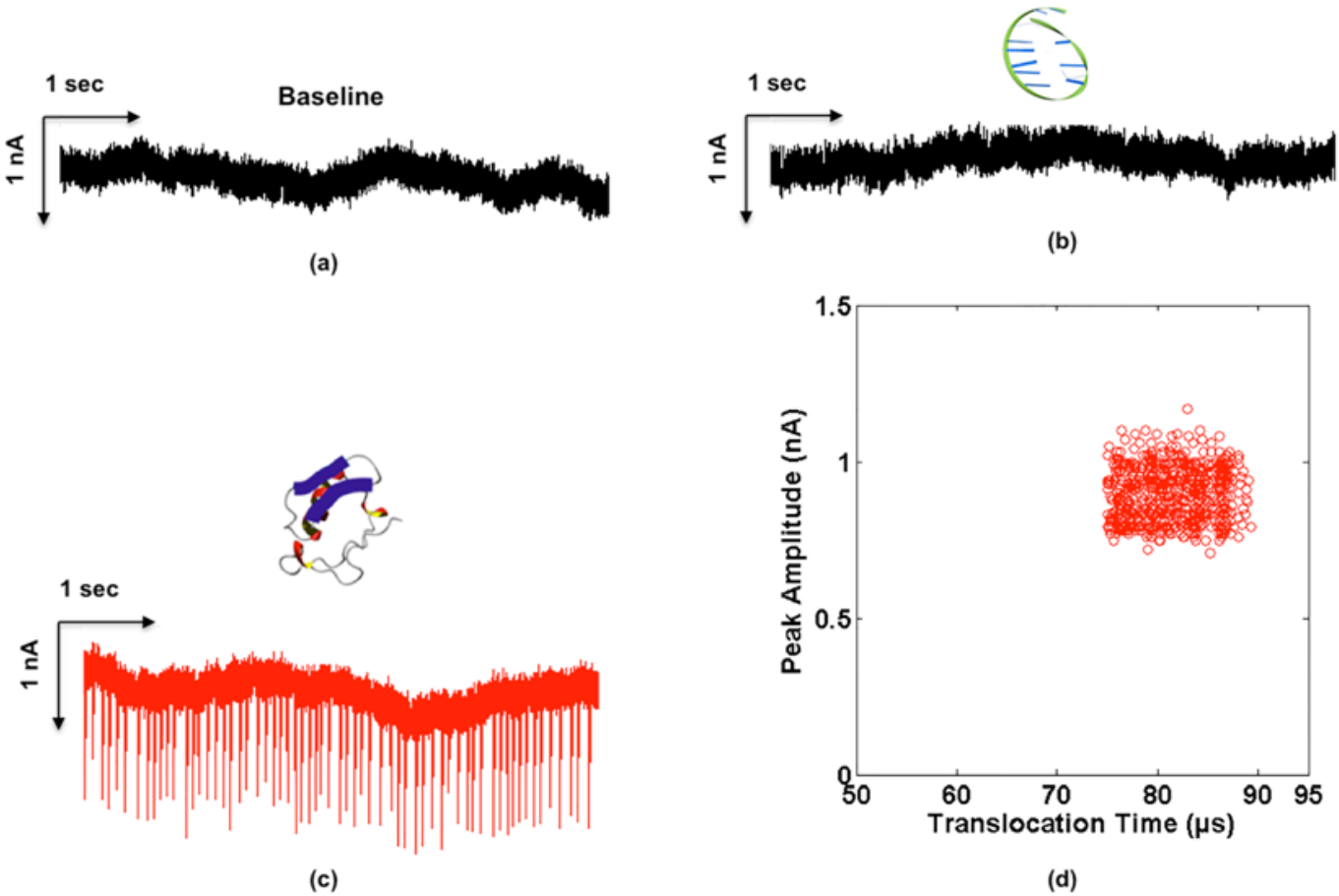

Figure 2 Snapshots of the nanopore current for 10 seconds duration for (a) Baseline, translocation of (b) Anti-EGFR aptamer (unbound only) (c) EGFR (unbound only) and (d) Scatter plot of the translocation time versus peak amplitude of the registered pulses for EGFR translocation through 40 nm nanopore at 50 mV. The registered pulses for EGFR translocation are consistent and form only one cluster of event population on the plot.

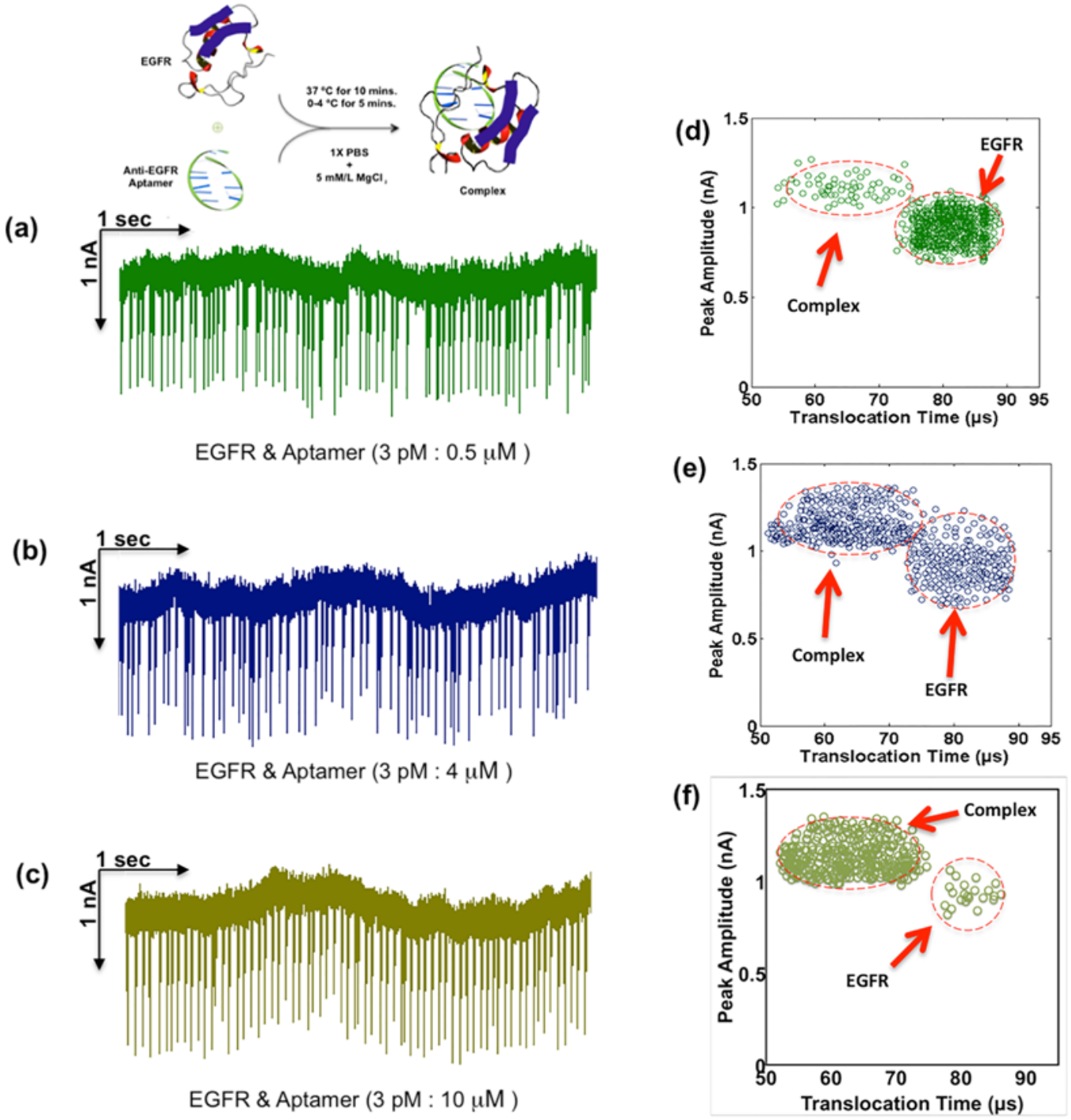

Figure 3 Snapshots of the ionic current trace for 10 seconds of the EGFR (3 pM) translocation when incubated with aptamer at (a) 0.5 μM (b) 4 μM and (c) 10 μM. The scatter plots show the translocation behavior of EGFR (3 pM) when incubated with aptamer at (d) 0.5 μM (e) 4 μM and (f) 10 μM. Two populations are visible: One with higher translocation time corresponds to the translocation of unbound EGFR, and second with shorter translocation time corresponds to complex's translocation.

In the first experiment with the complex translocation, there were plenty of unbound EGFR molecules present in the sample (Figure 3(d)). The number of unbound EGFR reduced as the aptamer concentration increased and ultimately very few unbound EGFR molecules were left (Figure 3(f)).

One might think that the second type of events can be associated with the translocation of free floating anti-EGFR aptamers in the solution. To rule this out, another experiment was carried out to record pulses for the translocation of anti-EGFR aptamer alone through the same nanopore. For this purpose, anti-EGFR aptamer was introduced into the negative side of the nanopore and no current blockage events were observed for this case (Figure 2(b)). There can be multiple reasons for that,the strongest being that a 40 nm nanopore is too large to detect the translocation of aptamer (few nanometers in size [43, 44]). Nanopore size should be close to the size of the target for detection [12, 13, 15]. In that case, even if aptamer were indeed translocating through the nanopore, their much smaller size than the nanopore

made it unlikely to register any pulses. Another possibility was that the charge on the aptamer was much smaller than the overall charge of EGFR. So even if 50 mV was enough to exert sufficient electrophoretic force on the EGFR to translocate through the nanopore, it was not sufficient to electrophorese aptamer alone through the nanopore. In that case, aptamer did not go through the nanopore at all and hence there were no pulses. Though this is a less likely case but it can not be ruled out completely. In any case, the point here is that, out of the two types of events that were observed for the translocation of EGFR after incubating it with aptamer, one was due to the translocation of EGFR alone and the other was due to the translocation of complex and not the free floating aptamer.

Finally, to check the specificity of this assay, experiment was repeated with human α-thrombin protein instead of EGFR. First, thrombin was translocated through a 40 nm wide and 40 nm thick nanopore at 50 mV. Figure 4(a) shows the current trace for thrombin translocation for 10 s duration. The average translocation time and average peak amplitude of the registered pulses from thrombin translocation were determined to be 68 ± 3.17 μs and 0.5 ± 0.15 nA, respectively. Thrombin (10.8 pM) was then incubated with anti-EGFR aptamer (10 μM) and sample was run through the same nanopore at 50 mV.

This time again, only one type of pulses were observed that were exact replica of those observed for thrombin only (without incubation with aptamer). The nanopore current trace for thrombin translocation after incubation with aptamer is shown in Figure 4(b). Figures 4(c) and 4(d) show the scatter plots of the events recorded by the translocation of thrombin-only and thrombin+anti-EGFR aptamer complex, respectively. The two populations are exactly the same indicating that thrombin translocation profile remained same before and after incubation with aptamer. This is because no aptamer attached to the thrombin and thus no thrombin-aptamer complexes were formed.

The dynamics of protein translocation, in general, through bare as well as chemically-modified solid-state nanopores and the forces involved in this process have already been explored through simulations and experiments [14, 21, 34, 37, 45-48]. EGFR translocation through the nanopore is not different from other proteins. At a pH of 8.2, carboxylic groups in EGFR molecules have negative charge whereas amines are protonated i.e. they attain positive charge. The isoelectric point (pI) for EGFR is 6.7 and at our buffer solution's pH the net charge on EGFR molecule is negative [49]. Due to this charge, after applying biasing voltage, electrophoretic force

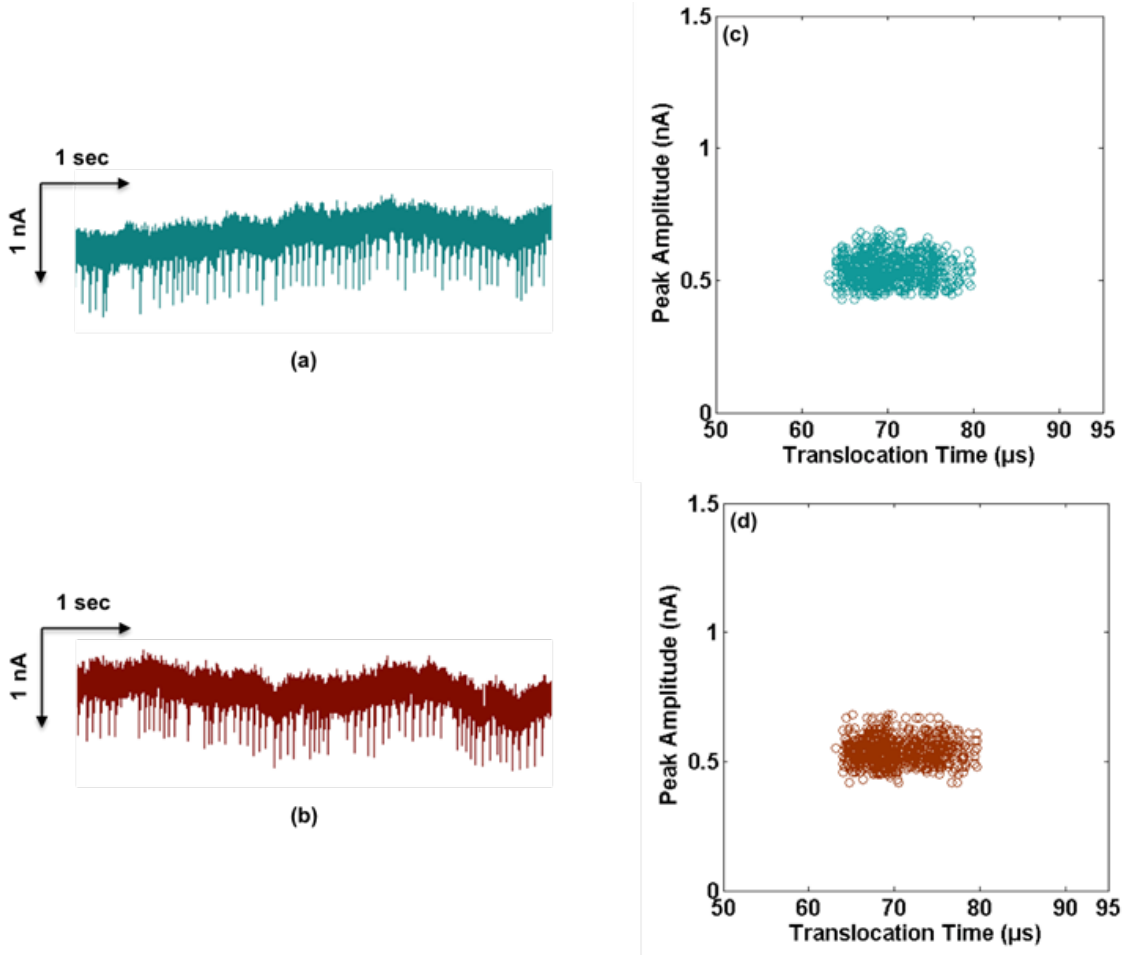

Figure 4 Snapshots of the nanopore ionic current traces for 10 seconds for the translocation of (a) Thrombin (b) Thrombin (11 pM) incubated with 10 pM of EGFR aptamer. Scatter plots of the registered pulses for the translocation of (c) Thrombin (d) Thrombin incubated with 10 pM EGFR aptamer.

(EP) pushes the EGFR molecules towards the positive electrode in the *other* compartment [50]. The velocity of this moving molecule can be calculated using Smoluchowski's equation [51, 52]: $\nu_{EP} = (\varepsilon/\eta)\zeta_{pro}.E$ where 'ν_{EP}' is the electrophoretic velocity of EGFR molecule, 'ε' is the dielectric constant, 'η' is the solution viscosity, 'ζ_{pro}' is the zeta potential for protein molecule and 'E' is the electric field. Electroosmotic flow (EO) in the electrolyte also affects the dynamics of the EGFR movement in nanopores. In some cases, EO can also cause a reverse flow of the proteins [47] i.e. negatively charged protein molecules will start moving towards the negative side, opposite to the EP. Reverse flow of the EGFR molecule was not observed in the experiments that meant that EO was either in the direction of EP or even if it was opposite to EP, it was not sufficient to counteract the EP. EP solely was dominant factor in governing EGFR direction of flow.

The overall translocation process can be split into two stages; (1) Capture step, and (2) Actual translocation through the nanopore. For a 40 nm pore, the capture of EGFR molecule will be diffusion controlled as opposed to the barrier-limited case. The dynamics of this diffusion controlled capture step can be calculated with the Smoluchowski's diffusion equation [40, 51-53]: $J = 2\pi cDr_p$, where 'J' is the rate at which the EGFR arrives at the nanopore entrance, 'c' is the bulk analyte concentration, 'D' is the diffusion constant and 'r_p' is the nanopore radius. Once EGFR has entered the nanopore, the translocation depends upon the zeta potential of the EGFR molecule and of the nanopore [50]. Cressiot *et al*. simulated the interaction of proteins with nanopore walls formed by focused ion beam (FIB) as well as TEM. They found that due to the absence of dangling atoms [54] and rearrangement of silica in nanopores formed by TEM, the interaction between proteins and nanopore walls was very weak [48]. Blockage time, $t_b = L/\nu_{EP}$ ('L' is nanopore channel length) is a function of the applied voltage [48] as well as the charge of the translocating species [19, 47]. Increasing either of these would increase the EP on the EGFR molecules and hence will decrease the blockage time and vice versa. At fixed applied bias of 50 mV, the pulses were pretty consistent in their widths i.e. translocation time or blockage time for EGFR translocation. Coagulation of molecules, if present, would have either blocked the nanopore completely or much longer translocation times would have been present [45]. However, none of such events were observed so it can be concluded that no EGFR coagulation occurred under these experimental conditions. Concurrent translocations of multiple EGFR molecules were observed though, but these events were very few and were mathematically discarded from the analysis. From single EGFR translocation events, very consistent pulse depths were observed. This was a clear indication of the uniform excluded volume of the EGFR molecules.

The specificity of anti-EGFR aptamer for EGFR and their attachment chemistry is quite well established [35, 36, 55]. When EGFR was incubated with the aptamer, they formed a complex with 1:1 stoichiometry. The estimated pI for aptamer was 5.5, at pH 8.2 it had almost the same charge as that of the EGFR. The attachment of EGFR with aptamer enhanced the overall charge of the complex. This also increased the mass of the complex than just EGFR alone. These changes influenced the overall dynamics of the complex translocation through the nanopore and made the translocation profile of complex different from that of EGFR. The additional charge of the complex very well explains the faster translocation of the complex through the nanopore. One might argue here that due to the additional mass it might be possible that the complex actually moved slower than the EGFR. However this was not the dominant factor in determining the translocation profile of the complex [37]. The overall change in charge was much more than the overall change in mass after the binding of aptamer with EGFR. That is why much more shift in the translocation time was observed than the peak amplitudes between the pulses associated with complex and EGFR-only translocation.

The shifting of the EGFR translocation behavior, as the molar concentration of aptamer increased, can be explained again with Smoluchowski's diffusion equation. According to this equation, the capture rate 'J' increases by increasing the analyte concentration 'c' in the solution. In Figure 3(d), the event rate is low for complex and higher for EGFR but as we increased the aptamer molar concentration, many more complexes were formed causing the event rate for them to shoot up (Figures 3(e) and 3(f)). No complexes were formed with thrombin and the translocation profile remained the same as before when no aptamer was involved.

The nanopores depicted a very selective and sensitive framework for label-free detection of EGFR from a sample. The use of bare nanopore made the process very simple and provided much more flexibility in the choice of nanopore size, unlike functionalized nanopore in which the ligand would be tethered inside the nanopore walls and the target must interact with the nanopore walls [37]. A functionalized nanopore is usable for one type of target and functionalization itself is a time consuming and labor extensive process. The use of bare nanopore with ligands to bind specific targets in solution increases the usability of the device since the same device can be used for multiple targets. There are no stringent limitations on the size of the nanopore as well.

III. MATERIALS AND METHODS

Materials: Recombinant Human EGFR/ErbB1 Fc Chimera, CF (EGFR ~134 KDa) was purchased from R&D Systems and human α-thrombin (Thrombin ~37 KDa) was purchased from Abcam, plc. Anti-EGFR aptamer had the sequence:

GGGCGCUCCGACCUUAGUCUCUGUGCCGCUAUAAUGC ACGGAUUUAAUCGCCGUAGAAAAGCAUGUCAAAGCCG GAACCGUGUAGCACAGCAGAGAAUUAAAUGCCCGCCA UGACCAG [36, 56]. All other chemicals were obtained from Sigma-Aldrich unless specified otherwise.

Nanopore Fabrication and Electrical Measurements: The nanopore of 40 nm diameter and 40 nm length (Figure 1(a)) was used for all the translocation experiments. The nanopore was drilled in a thin suspended silicon nitride membrane by focusing an electron beam of a TEM. Nanopore diameter was controlled by the exposure time [57]. The detailed fabrication process for membranes is reported elsewhere [58]. The nanopore chip was sandwiched between two PDMS gaskets that were further sandwiched between two Teflon blocks that contained the electrophoresis buffer solution. Protein unfolding has strong dependence on the applied voltage [21, 48]. To keep proteins in their native states and to avoid any unfolding all the translocation experiments were done at a very low voltage i.e. 50 mV. For current measurement and to apply the voltage, Ag/AgCl electrodes were immersed in the buffer solution and were connected to Axopatch 200B through the headstage. Current recording was done at a bandwidth of 250 kHz whereas filtering was done at 100 kHz with a lowpass Bessel filter. A custom made MATLAB routine [59] was used for the analysis of the data. The *t*-test was done for statistical analysis.

In-solution Binding of EGFR and Aptamer: EGFR and anti-EGFR aptamer were mixed in the binding buffer (Figure 2(c)). The binding buffer constituted of 1X PBS and 5 mM/l $MgCl_2$. Three separate mixtures were prepared by mixing EGFR and anti-EGFR aptamer in different concentrations. In mixture 1, 8 µl of 50 ng/µl (3 pM) EGFR was mixed with 0.5 µM aptamer. In mixture 2 and 3, EGFR concentration was kept same as mixture 1 but aptamer concentration was 4 µM and 10 µM, respectively. The mixtures were incubated at 37 °C for 10 minutes and then placed in freezer (0-4 °C) for 5 minutes. The details on binding dynamics have been explained before [36]. For control experiments, 8 µl of human α-thrombin protein at 50 ng/µl (11 pM) concentration was also mixed with anti-EGFR aptamer (10 µM) and was incubated first at 37 °C for 10 minutes and then at 0-4 °C for 5 minutes.

IV. CONCLUSIONS

In summary, the use of nanopore based resistive-pulse sensors for rapid and reliable detection of EGFR has been presented. Due to high single molecule sensitivity of nanopore sensors, a very small amount of EGFR has been detected. EGFR overexpression, though an early biomarker for different types of cancers, have not yet been utilized properly for early cancer detection. Available methods are either not sensitive enough to detect very small changes in the quantities of EGFR or require elaborate preparation. The simple preprocessing steps make the presented approach suitable for lab settings in resource-poor regions and may provide cheap cancer screening options. The methodology can be further expanded for the detection of other biomarkers as well if there are matching ligands available. Additionally this technique can be used to determine the affinity of the aptamer-protein complex as well.

V. ACKNOWLEDGEMENT

We thank Raja Raheel Khanzada for his help with the graphics of this paper. We would also like to thank Dr. Andrew D. Ellington from the University of Texas at Austin for providing us the aptamer molecules. This work was supported by grant ECCS-1201878 from National Science Foundation, USA.

VI. REFERENCES

1. Pepe MS, Etzioni R, Feng Z, Potter JD, Thompson ML, Thornquist M, Winget M, Yasui Y. Phases of biomarker development for early detection of cancer, Journal of the National Cancer Institute. 93(2001) 1054-61.
2. Wulfkuhle JD, Liotta LA, Petricoin EF. Proteomic applications for the early detection of cancer, Nature Reviews Cancer. 3(2003)267-75.
3. Rusling JF. Multiplexed electrochemical protein detection and translation to personalized cancer diagnostics, Analytical Chemistry. 85(2013)5304-10.
4. Gabos Z, Sinha R, Hanson J, Chauhan N, Hugh J, Mackey JR, Abdulkarim B. Prognostic significance of human epidermal growth factor receptor positivity for the development of brain metastases after newly diagnosed breast cancer, Journal of Clinical Oncology: Official Journal of the American Society of Clinical Oncology. 24(2006)5658-63.
5. Mak MP, William WN, Jr. Targeting the epidermal growth factor receptor for head and neck cancer chemoprevention, Oral oncology. 50(2014)918-23.
6. Maheswaran S, Sequist LV, Nagrath S, Ulkus L, Brannigan B, Collura CV, Inserra E, Diederichs S, Iafrate AJ, Bell DW, et al. Detection of mutations in EGFR in circulating lung-cancer cells, The New England Journal of Medicine. 359(2008)366-77.
7. Voldborg BR, Damstrup L, Spang-Thomsen M, Poulsen HS. Epidermal growth factor receptor (EGFR) and EGFR mutations, function and possible role in clinical trials, Annals of Oncology: Official Journal of the European Society for Medical Oncology/ESMO. 8(1997)1197-206.
8. Mendelsohn J, Baselga J. Epidermal growth factor receptor targeting in cancer, Seminars

in Oncology. 33(2006)369-85.
9. Quaranta M, Divella R, Daniele A, Di Tardo S, Venneri MT, Lolli I, Troccoli G. Epidermal growth factor receptor serum levels and prognostic value in malignant gliomas, Tumori. 93(2007)275-80.
10. Nam JM, Thaxton CS, Mirkin CA. Nanoparticle-based bio-bar codes for the ultrasensitive detection of proteins, Science. 301(2003)1884-6.
11. Gubala V, Harris LF, Ricco AJ, Tan MX, Williams DE. Point of care diagnostics: status and future, Analytical Chemistry. 84(2012)487-515.
12. Venkatesan BM, Bashir R. Nanopore sensors for nucleic acid analysis. Nature Nanotechnology. 6(2011)615-24.
13. Bell NA, Engst CR, Ablay M, Divitini G, Ducati C, Liedl T, Keyser UF. DNA origami nanopores, Nano Letters. 12(2012)512-7.
14. Wei R, Gatterdam V, Wieneke R, Tampe R, Rant U. Stochastic sensing of proteins with receptor-modified solid-state nanopores, Nature Nanotechnology. 7(2012)257-63.
15. Iqbal SM, Akin D, Bashir R. Solid-state nanopore channels with DNA selectivity, Nature Nanotechnology. 2(2007)243-8.
16. Soni GV, Dekker C. Detection of nucleosomal substructures using solid-state nanopores, Nano Letters. 12(2012)3180-6.
17. Niedzwiecki DJ, Iyer R, Borer PN, Movileanu L. Sampling a biomarker of the human immunodeficiency virus across a synthetic nanopore, ACS Nano. 7(2013)3341-50.
18. Chen P, Mitsui T, Farmer DB, Golovchenko J, Gordon RG, Branton D. Atomic Layer Deposition to Fine-Tune the Surface Properties and Diameters of Fabricated Nanopores, Nano Letters. 4(2004)1333-7.
19. Fologea D, Ledden B, McNabb DS, Li J. Electrical characterization of protein molecules by a solid-state nanopore, Applied Physics Letters. 91(2007)539011-3.
20. Talaga DS, Li J. Single-molecule protein unfolding in solid state nanopores, Journal of the American Chemical Society. 131(2009)9287-97.
21. Rodriguez-Larrea D, Bayley H. Multistep protein unfolding during nanopore translocation, Nature Nanotechnology. 8(2013)288-95.
22. Uram JD, Ke K, Hunt AJ, Mayer M. Submicrometer pore-based characterization and quantification of antibody-virus interactions, Small. 2(2006)967-72.
23. Ali M, Bayer V, Schiedt B, Neumann R, Ensinger W. Fabrication and functionalization of single asymmetric nanochannels for electrostatic/hydrophobic association of protein molecules, Nanotechnology. 19(2008)485711.
24. Majd S, Yusko EC, Billeh YN, Macrae MX, Yang J, Mayer M. Applications of biological pores in nanomedicine, sensing, and nanoelectronics, Current Opinion in Biotechnology. 21(2010)439-76.
25. Bayley H, Cremer PS. Stochastic sensors inspired by biology, Nature. 413(2001)226-30.
26. Liu A, Zhao Q, Guan X. Stochastic nanopore sensors for the detection of terrorist agents: current status and challenges, Analytica Chimica Acta. 675(2010)106-15.
27. Maglia G, Heron AJ, Stoddart D, Japrung D, Bayley H. Analysis of single nucleic acid molecules with protein nanopores, Methods in Enzymology. 475 (2010) 591-623.
28. Nivala J, Marks DB, Akeson M. Unfoldase-mediated protein translocation through an alpha-hemolysin nanopore, Nature Biotechnology. 31(2010)247-50.
29. Movileanu L. Interrogating single proteins through nanopores: challenges and opportunities, Trends in Biotechnology. 27(2009)333-41.
30. Hernandez-Ainsa S, Keyser UF. DNA origami nanopores: developments, challenges and perspectives, Nanoscale. 6(2014)14121-32.
31. Payet L, Martinho M, Pastoriza-Gallego M, Betton JM, Auvray L, Pelta J, Mathe J. Thermal unfolding of proteins probed at the single molecule level using nanopores, Analytical Chemistry. 84(2012)4071-6.
32. Han A, Creus M, Schurmann G, Linder V, Ward TR, de Rooij NF, Staufer U. Label-free detection of single protein molecules and protein-protein interactions using synthetic nanopores, Analytical Chemistry. 80(2008)4651-8.
33. Howorka S, Siwy Z. Nanopore analytics: sensing of single molecules, Chemical Society Reviews. 38(2009)2360-84.
34. Rotem D, Jayasinghe L, Salichou M, Bayley H. Protein detection by nanopores equipped with aptamers, Journal of the American Chemical Society. 134(2012)2781-7.
35. Bunka DH, Stockley PG. Aptamers come of age - at last,Nature Reviews Microbiology. 4(2006)588-96.
36. Wan Y, Mahmood MA, Li N, Allen PB, Kim YT, Bachoo R, Ellington AD, Iqbal SM. Nanotextured substrates with immobilized aptamers for cancer cell isolation and cytology, Cancer. 118(2012)1145-54.
37. Mahmood MA, Ali W, Adnan A, Iqbal SM. 3D structural integrity and interactions of single-stranded protein-binding DNA in a functionalized nanopore, The Journal of Physical Chemistry B. 118(2014)5799-806.
38. He Y, Tsutsui M, Scheicher RH, Fan C, Taniguchi M, Kawai T. Mechanism of how salt-gradient-induced charges affect the translocation of DNA molecules through a nanopore, Biophysical Journal. 105(2013)776-82.
39. Kowalczyk SW, Dekker C. Measurement of the docking time of a DNA molecule onto a solid-state nanopore, Nano Letters. 12(2012)4159-63.
40. Plesa C, Kowalczyk SW, Zinsmeester R,

Grosberg AY, Rabin Y, Dekker C. Fast translocation of proteins through solid state nanopores, Nano Letters. 13(2013)658-63.
41. Ho C, Qiao R, Heng JB, Chatterjee A, Timp RJ, Aluru NR, Timp G. Electrolytic transport through a synthetic nanometer-diameter pore, Proceedings of the National Academy of Sciences of the United States of America. 102(2005)10445-50.
42. Kowalczyk SW, Kapinos L, Blosser TR, Magalhaes T, van Nies P, Lim RY, Dekker C. Single-molecule transport across an individual biomimetic nuclear pore complex, Nature Nanotechnology. 6(2011)433-8.
43. Zhang H, Li XF, Le XC. Tunable aptamer capillary electrophoresis and its application to protein analysis, Journal of the American Chemical Society. 130(2008)34-5.
44. van den Hout M, Skinner GM, Klijnhout S, Krudde V, Dekker NH. The passage of homopolymeric RNA through small solid-state nanopores, Small. 7(2011)2217-24.
45. Yusko EC, Johnson JM, Majd S, Prangkio P, Rollings RC, Li J, Yang J, Mayer M. Controlling protein translocation through nanopores with bio-inspired fluid walls, Nature Nanotechnology. 6(2011)253-60.
46. Kowalczyk SW, Hall AR, Dekker C. Detection of local protein structures along DNA using solid-state nanopores, Nano Letters. 10(2010)324-8.
47. Firnkes M, Pedone D, Knezevic J, Doblinger M, Rant U. Electrically facilitated translocations of proteins through silicon nitride nanopores: conjoint and competitive action of diffusion, electrophoresis, and electroosmosis, Nano Letters. 10(2010)2162-7.
48. Cressiot B, Oukhaled A, Patriarche G, Pastoriza-Gallego M, Betton JM, Auvray L, Muthukumar M, Bacri L, Pelta J. Protein transport through a narrow solid-state nanopore at high voltage: experiments and theory, ACS Nano. 6(2012)6236-43.
49. Ceresa BP, Peterson JL. Cell and molecular biology of epidermal growth factor receptor, International Review of Cell and Molecular Biology. 313 (2014) 145-78.
50. Lu B, Hoogerheide DP, Zhao Q, Yu D. Effective driving force applied on DNA inside a solid-state nanopore, Physical Review E, Statistical, Nonlinear, and Soft Matter Physics. 86(2012)011921.
51. Peters B, Bolhuis PG, Mullen RG, Shea JE. Reaction coordinates, one-dimensional Smoluchowski equations, and a test for dynamical self-consistency, The Journal of Chemical Physics. 138(2013)054106.
52. Egorova EM. The validity of the Smoluchowski equation in electrophoretic studies of lipid membranes, Electrophoresis. 15(1994)1125-31.
53. Family F, Meakin P, Deutch JM. Kinetics of coagulation with fragmentation: Scaling behavior and fluctuations, Physical Review Letters. 57(1986)727-30.
54. Cruz-Chu ER, Aksimentiev A, Schulten K. Ionic Current Rectification Through Silica Nanopores, The Journal of Physical Chemistry C, Nanomaterials and Interfaces. 113(2009)1850.
55. Wan Y, Tan J, Asghar W, Kim YT, Liu Y, Iqbal SM. Velocity effect on aptamer-based circulating tumor cell isolation in microfluidic devices, The Journal of Physical Chemistry B. 115(2011)13891-6.
56. Wan Y, Liu Y, Allen PB, Asghar W, Mahmood MA, Tan J, Duhon H, Kim YT, Ellington AD, Iqbal SM. Capture, isolation and release of cancer cells with aptamer-functionalized glass bead array, Lab On a Chip. 12(2012)4693-701.
57. Fischbein MD, Drndic M. Sub-10 nm device fabrication in a transmission electron microscope, Nano Letters. 7(2007)1329-37.
58. Asghar W, Ilyas A, Deshmukh RR, Sumitsawan S, Timmons RB, Iqbal SM. Pulsed plasma polymerization for controlling shrinkage and surface composition of nanopores, Nanotechnology. 22(2011)285304.
59. Billo JA, Asghar W, Iqbal SM. An Implementation for the Detection and Analysis of Negative Peaks in an Applied Current Signal across a Silicon Nanopore, Micro- and Nanotechnology Sensors, Systems, and Applications III. 8031 (2011) 80312T.